ADVANCES IN ATMOSPHERIC SCIENCES, VOL. 34, DECEMBER 2017, 1381–1394

• **Original Paper** •

Sensitivity of Potential Evapotranspiration Estimation to the Thornthwaite and Penman–Monteith Methods in the Study of Global Drylands

Qing YANG*[1], Zhuguo MA[1,2], Ziyan ZHENG[1], and Yawen DUAN[1,2]

[1]*Key Laboratory of Regional Climate–Environment for Temperate East Asia, Institute of Atmospheric Physics, Chinese Academy of Sciences, Beijing* 100029*, China*

[2]*University of Chinese Academy of Sciences, Beijing* 100049*, China*

(Received 19 December 2016; revised 28 April 2017; accepted 16 Jun 2017)

ABSTRACT

Drylands are among those regions most sensitive to climate and environmental changes and human-induced perturbations. The most widely accepted definition of the term dryland is a ratio, called the Surface Wetness Index (SWI), of annual precipitation to potential evapotranspiration (PET) being below 0.65. PET is commonly estimated using the Thornthwaite (PET_Th) and Penman–Monteith equations (PET_PM). The present study compared spatiotemporal characteristics of global drylands based on the SWI with PET_Th and PET_PM. Results showed vast differences between PET_Th and PET_PM; however, the SWI derived from the two kinds of PET showed broadly similar characteristics in the interdecadal variability of global and continental drylands, except in North America, with high correlation coefficients ranging from 0.58 to 0.89. It was found that, during 1901–2014, global hyper-arid and semi-arid regions expanded, arid and dry sub-humid regions contracted, and drylands underwent interdecadal fluctuation. This was because precipitation variations made major contributions, whereas PET changes contributed to a much lesser degree. However, distinct differences in the interdecadal variability of semi-arid and dry sub-humid regions were found. This indicated that the influence of PET changes was comparable to that of precipitation variations in the global dry–wet transition zone. Additionally, the contribution of PET changes to the variations in global and continental drylands gradually enhanced with global warming, and the Thornthwaite method was found to be increasingly less applicable under climate change.

Key words: potential evapotranspiration, global drylands, Thornthwaite, Penman–Monteith

Citation: Yang, Q., Z. G. Ma, Z. Y. Zheng, and Y. W. Duan, 2017: Sensitivity of potential evapotranspiration estimation to the Thornthwaite and Penman–Monteith methods in the study of global drylands. *Adv. Atmos. Sci.*, **34**(12), 1381–1394, https://doi.org/10.1007/s00376-017-6313-1.

1. Introduction

Drought is the world's costliest natural disaster. It manifests over multiple temporal and spatial scales, and can have considerable influence on ecosystems, economies and society (Heim Jr, 2002). To monitor, detect and quantify drought, many drought indices have been developed (Heim Jr, 2002; Keyantash and Dracup, 2002; Mishra and Singh, 2010; Valipour, 2013). Precipitation is the most important factor regarding water availability in land hydrological systems, and thus various measures of precipitation over a given period of time are incorporated in meteorological drought definitions (Heim Jr, 2002). Additionally, it has been generally recognized that the capabilities of drought indices that consider potential evapotranspiration (PET) to depict land water conditions are better (Vicente-Serrano et al., 2012).

PET represents the maximum amount of water capable of being lost through evaporation from the soil surface and via transpiration at the canopy level under a given set of atmospheric conditions, assuming complete vegetation cover of the ground and an adequate water supply (Food and Agriculture Organization of the United Nations, 2008). Compared with actual evapotranspiration, PET can be more easily estimated from meteorological data and provides a reasonable representation for surface evapotranspiration to some extent (Valipour et al., 2017); especially in humid areas, PET tends to equal to actual evapotranspiration (Gao et al., 2007). Currently, many methods are available for the calculation of PET (e.g. Thornthwaite, 1948; Shuttleworth and Wallace, 1985; Allen et al., 1994a, 1994b; Hargreaves and Allen, 2003; Tegos et al., 2015; McMahon et al., 2016; Valipour et al., 2017). For instance, Thornthwaite (1948) proposed a method to estimate PET (known as the Thornthwaite method) based only on daily averaged temperature and the maximum amount of sunshine duration, which is calculated based on latitude.

* Corresponding author: Qing YANG
Email: yangqing@tea.ac.cn

The Penman–Monteith equation is a physically based approach that considers wind speed, humidity and solar and longwave radiation in addition to temperature (Allen et al., 1994a, 1994b). A two-source PET model (Yuan and Quiring, 2014), which is also known as the Shuttleworth–Wallace model (Shuttleworth and Wallace, 1985; Zhou et al., 2008), is considered an improvement over the Penman–Monteith equation because it addresses the radiation balance at the canopy level and the soil surface separately.

The choice of proper methods for the calculation of PET has recently received considerable attention and has sparked notable controversy (e.g. Trenberth et al., 2014; Tegos et al., 2015; Rezaei et al., 2016; Zhang et al., 2016; Valipour et al., 2017; Feng et al., 2017). Global drought trends under climate change are still a matter of debate, caused by the differences between the Thornthwaite-based and Penman–Monteith-based PET (Sheffield et al., 2012; Dai, 2013; van der Schrier et al., 2013; Trenberth et al., 2014; Yuan and Quiring, 2014). The Palmer Drought Severity Index (PDSI; Palmer, 1965) is calculated using a complex water budget system based on precipitation, temperature and the soil characteristics of the site. It has been found to be not very sensitive to different methods for calculating PET in the formulation of the PDSI (Dai, 2011; van der Schrier et al., 2011; Yuan and Quiring, 2014). Consequently, Dai (2011) reported that when the PDSI is calculated using either the Thornthwaite or Penman–Monteith method for calculating PET, there are no significant differences in global drought patterns, and significant global drying trends can be found with both approaches. However, Sheffield et al. (2012) suggested there has been little change in global drought over the past 60 years when using the Penman–Monteith-based PDSI, and that the global drying trend revealed by the Thornthwaite-based PDSI is overestimated.

Drylands are considered to be areas where average rainfall is less than the potential moisture losses though evapotranspiration, and they are among those regions most sensitive to climate and environmental changes and human-induced perturbations (Reynolds et al., 2007; Huang Jr, 2016a). Understanding the response of drylands to climate change is essential for developing adaptation and mitigation strategies, and thus has become a subject of widespread concern (Hulme et al., 1992; Lioubimtseva and Henebry, 2009; Feng and Fu, 2013). It has been demonstrated that global drylands expanded remarkably during 1948 to 2005, especially in Africa and Eurasia (Ma and Fu, 2007). In China, the boundary between arid and semi-arid land has noticeably expanded eastwards and southwards in the past 100 years, and dryland expansion in northern China is evident because of decreasing precipitation, together with increasing evaporation (Ma and Fu, 2003, 2005, 2006; An et al., 2014; Li et al., 2015).

Most climatological studies on dryland, as above (e.g. Sherwood and Fu, 2014), tend to be based on a common definition of the term "drylands". This definition, which is provided by the World Atlas of Desertification (UNEP, 1992), employs a ratio of annual precipitation to PET, called the Surface Wetness Index (SWI; Hulme et al., 1992; UNEP, 1992). Various methods for the calculation of PET have been used in the SWI; for instance, the Thornthwaite method (Ma and Fu, 2003, 2005, 2006, 2007) and Penman–Monteith method (Liu and Ma, 2007; Feng and Fu, 2013; Li et al., 2015; Huang Jr, 2016a). Of note is that, different from the PDSI, the SWI does not feature any parametrization, standardization or post-processing, and is therefore certainly affected by different estimates of PET. Consequently, notable differences in the spatiotemporal characteristics of global drylands, attributable to different estimates of PET, are expected. However, sensitivity of the SWI to different methods for the calculation of PET, in the study of the spatial distribution and temporal evolution of global drylands, has yet to be investigated. Therefore, the present study aimed to quantitatively identify the differences in the spatiotemporal variabilities of global drylands between the Thornthwaite and Penman–Monteith parameterizations for PET.

The paper is organized as follows: Section 2 introduces the data and method. This is followed by a comparison of the PET values derived using the Thornthwaite and Penman–Monteith methods in section 3. Section 4 presents the spatiotemporal characteristics of global drylands defined by the SWI with the two estimates of PET. A discussion and conclusions are summarized in section 5.

2. Data and methods

2.1. *Data*

Several datasets were used in this study: (1) Global land monthly precipitation, air temperature, cloud cover, vapor pressure, and PET, from 1901 to 2014, with a high resolution of $0.5° \times 0.5°$, were obtained from the CRU TS3.23 (Harris et al., 2014). The PET was calculated using the Penman–Monteith formula, as developed and recommended by the Food and Agricultural Organization (FAO) (Allen et al., 1994a, 1994b). Because of its high reliability, this PET dataset has been used for the calculation of SPEIbase v2.4 (Vicente-Serrano et al., 2010a, 2010b; Beguería et al., 2014). (2) The Global Land Cover Map (GlobCover) for 2009, representing 22 land cover classes, with a horizontal resolution of 300 m, was obtained from the European Space Agency (Bontemps et al., 2011).

2.2. *Estimation of PET*

2.2.1. *Thornthwaite method*

Thornthwaite (1948) correlated monthly mean temperature with PET, as determined from the water balance, for valleys in the eastern USA, where there was a supply of surface water. Willmott et al. (1985) modified Thornthwaite's original approach slightly by introducing parameterization for a limited range of average air temperature T (Units: °C):

$$\mathrm{PET} = \begin{cases} 0 & T < 0 \\ 16\left(\dfrac{10T}{I}\right)^{\alpha} & 0 \leqslant T < 26.5 \\ -415.85 + 32.24T - 0.43T^2 & T \geqslant 26.5 \end{cases}, \quad (1)$$

where I is the heat index and α is estimated using an I-related third-order polynomial:

$$I = \sum_{i=1}^{12} \left(\frac{T}{5}\right)^{1.514} \qquad T > 0\ ; \tag{2}$$

$$\alpha = 0.49239 + 1.792\times10^{-2} I - 7.71\times10^{-5} I^2 + 6.75\times10^{-7} I^3\ . \tag{3}$$

To account for the variability of day h and month length θ, PET is adjusted to

$$\mathrm{PET} = \mathrm{PET}\left(\frac{\theta}{30}\right)\left(\frac{h}{12}\right)\ . \tag{4}$$

Descriptions of each component in the above formulas are provided in Table 1.

2.2.2. *Penman–Monteith method*

The Penman–Monteith equation is a physically based method that uses a "big leaf" assumption. It defines a reference PET based on a hypothetical land cover, which closely resembles a clipped grass surface with uniform height (0.12 m), fixed surface resistance (70 s m^{-1}), and surface albedo (0.23) (Allen et al., 1994a, 1994b). In addition, water is abundantly available at the reference evapotranspiration rate. Here, the FAO Penman–Monteith equation is given as

$$\mathrm{PET} = \frac{0.408\Delta(R_\mathrm{n} - G) + \gamma \frac{900}{T+273.16} u_2 (e_\mathrm{s} - e_\mathrm{a})}{\Delta + \gamma(1 + 0.34u_2)}\ . \tag{5}$$

Definitions of the various components used in this formula are provided in Table 1.

2.3. *SWI*

The SWI, which is the ratio of the annual accumulated precipitation to PET, is also known as the Humidity Index (Hulme et al., 1992; UNEP, 1992) and the Aridity Index (Huang Jr, 2016a, 2016b):

$$\mathrm{SWI} = \frac{\sum_{i=1}^{12} P_i}{\sum_{i=1}^{12} \mathrm{PE}_i}\ , \tag{6}$$

Table 1. Parameters used in the Thornthwaite and Penman–Monteith methods.

Thornthwaite	Penman–Monteith
T, 2-m average air temperature (°C);	T, 2-m average air temperature (°C);
θ, the length of the month (days);	R_n, crop surface net radiation (MJ m^{-2} d^{-1});
Latitude, which is used for calculating the duration of daylight on the 15th day of the month;	G, soil heat flux (MJ m^{-2} d^{-1});
h (hour)	u_2, 2-m wind speed (m s^{-1});
	e_s, saturation vapor pressure (kPa);
	e_a, actual vapor pressure (kPa);
	Δ, slope of the vapor pressure curve (kPa $°C^{-1}$);
	γ, psychrometric constant (kPa $°C^{-1}$);
	900, coefficient for the reference crop;
	0.34, wind coefficient for the reference crop

where P_i and PE_i are the monthly precipitation and PET, respectively. Drylands are defined as regions where the SWI is below 0.65, including hyper-arid (SWI < 0.05), arid (0.05 ⩽ SWI < 0.20), semi-arid (0.20 ⩽ SWI < 0.50) and dry subhumid regions (0.50 ⩽ SWI < 0.65).

In this study, the PET estimated using the Thornthwaite and Penman–Monteith method is denoted as PET_Th and PET_PM, respectively. The SWI forced by the same precipitation amount but with the PET_Th or PET_PM is referred to as SWI_Th and SWI_PM, respectively.

2.4. *Method*

The Ensemble Empirical Mode Decomposition (EEMD) method (Huang and Wu, 2008; Wu and Huang, 2009) is a recently developed data-adaptive filter, which has been employed to decompose time series into various timescale components (Wu et al., 2011; Xia et al., 2013; Qian and Zhou, 2014). In this study, the EEMD method was used to decompose the annual time series of global drylands for the period 1901–2014 to obtain their multidecadal variability and nonlinear trends. The Student's t-test (Wilks, 2005) was used to calculate the significance of the difference between two time series.

3. Comparison of PET values

Figures 1a and b show distinct differences between the spatial distributions of PET_Th and PET_PM, with significant zonal characteristics (Fig. 1c). Compared with PET_PM, PET_Th was much lower in the subtropics, whereas it was much higher in the tropics and high northern latitudes.

As shown in Fig. 2, PET_Th and air temperature had similar zonal distributions, i.e., a unimodal distribution with a peak at approximately 10°N. However, PET_PM showed a bimodal distribution, with two peaks in the subtropics and a low in the tropics. Abundant convective clouds and precipitation in the tropics reduce solar radiation and vapor pressure deficit, resulting in low values of PET, whereas the subtropics are associated with the opposite conditions. Consequently, PET values in the tropics should be much lower than in the subtropics. This indicates that PET_PM is more reasonable and reliable than PET_Th; the latter overestimates PET in the tropics but underestimates it in the subtropics, because of the exclusion of cloud cover and vapor pressure deficit in the Thornthwaite parameterization. This result is consistent with that of van der Schrier et al. (2011), who investigated the dependence of the PDSI on the alternative Thornthwaite and Penman-Monteith methods for PET.

Despite the large differences in the spatial distributions, the interannual variabilities of PET_Th and PET_PM were quite similar. As shown in Fig. 3a, significant positive correlations between PET_Th and PET_PM were found in most areas. For example, regions with correlation coefficients above 0.8 were located in North Africa, Southern Europe, Central Asia, and the Brazilian highlands. However, the long-term trends of PET_PM differed from those of PET_Th. Figure 3b

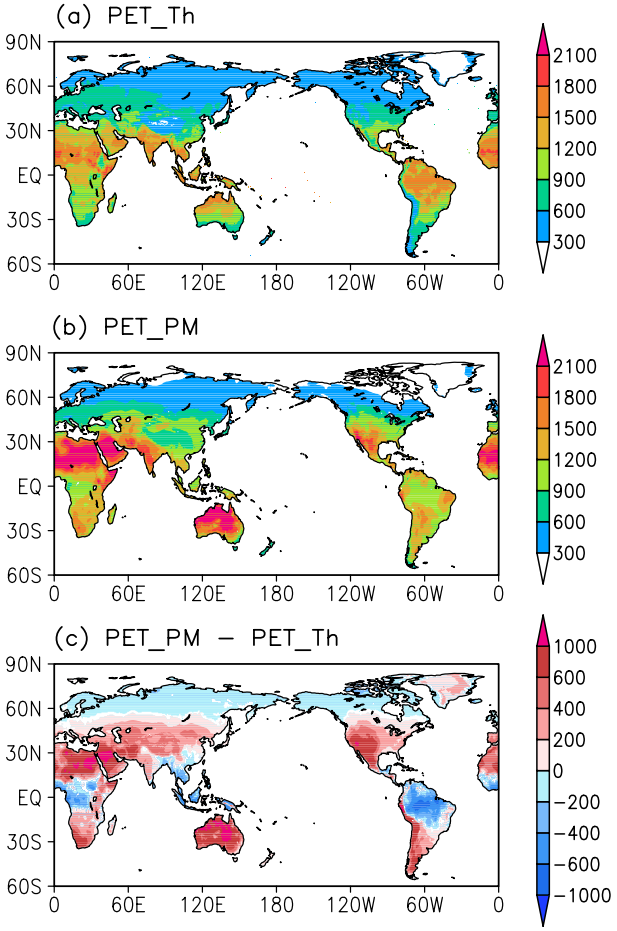

Fig. 1. Spatial distributions of average (1951–2014) annual accumulated PET (units: mm) using (a) Thornthwaite (PET_Th) and (b) Penman–Monteith (PET_PM) equations, and (c) their differences (PET_PM minus PET_Th). The shaded areas in (c) denote differences that are statistically significant at the 0.001 level.

shows regions with significant warming accounted for approximately 87% of the global land area, excluding Antarctica. Among these regions, approximately 87% of areas had significantly increasing PET_Th, while only around 54% of areas had significantly increasing PET_PM (Figs. 3c and d). This means that PET_Th increases with global warming, whereas the long-term trends of PET_PM are not determined by air temperature alone (Xu et al., 2006; Fu et al., 2009). Many studies have demonstrated a decrease in PET in many places throughout the world over the past 50 years (e.g., Roderick and Farquhar, 2002; Xu et al., 2006; Gao et al., 2006; Fu et al., 2009)—a trend that is associated with widespread decreases in solar radiation resulting from increasing cloud coverage and aerosol concentration (Roderick and Farquhar, 2002), wind speed (Gao et al., 2006), and vapor pressure deficit (Cong et al., 2009; Fu et al., 2009). Therefore, PET_PM shows a more reasonable long-term trend.

To elaborate on the temporal variabilities of the two types of PET, the regional-averaged PET and associated statistical information for northern South America, the USA, North Australia, and Central Asia are shown in Fig. 4 and Table 2. Considerable differences between PET_Th and PET_PM were evident in these regions, with differences ranging from −217.1 (northern South America) to 838.3 mm (North Australia). The long-term trends of PET were opposing, i.e., there was a significant increasing trend in PET_Th but a significant decreasing trend in PET_PM for the periods 1901–2014 and 1951–2014. In addition, the interannual variations of PET_Th and PET_PM over northern South America were markedly different, with a correlation coefficient of only 0.1.

4. Comparison of temporal and spatial characteristics of global drylands attributed to the two estimates of PET

4.1. *Variability in spatial distribution*

The spatial distributions of global drylands based on multi-year averages of SWI_ PM and SWI_Th are displayed in Fig. 5. Although the two patterns were broadly similar, the

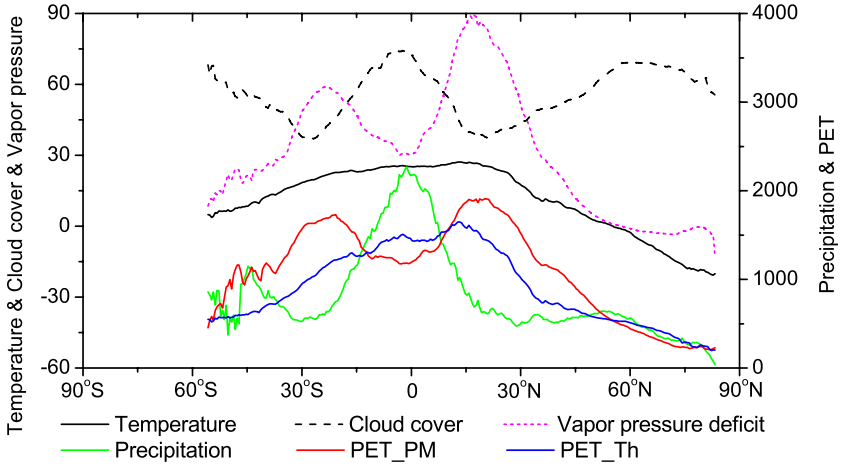

Fig. 2. Zonally averaged values of (left-hand axis) annual mean air temperature (units: °C), cloud cover (units: %) and vapor pressure deficit (×5; units: hPa), and (right-hand axis) annual accumulated precipitation, PET_Th and PET_PM (units: mm), for the period 1951–2014.

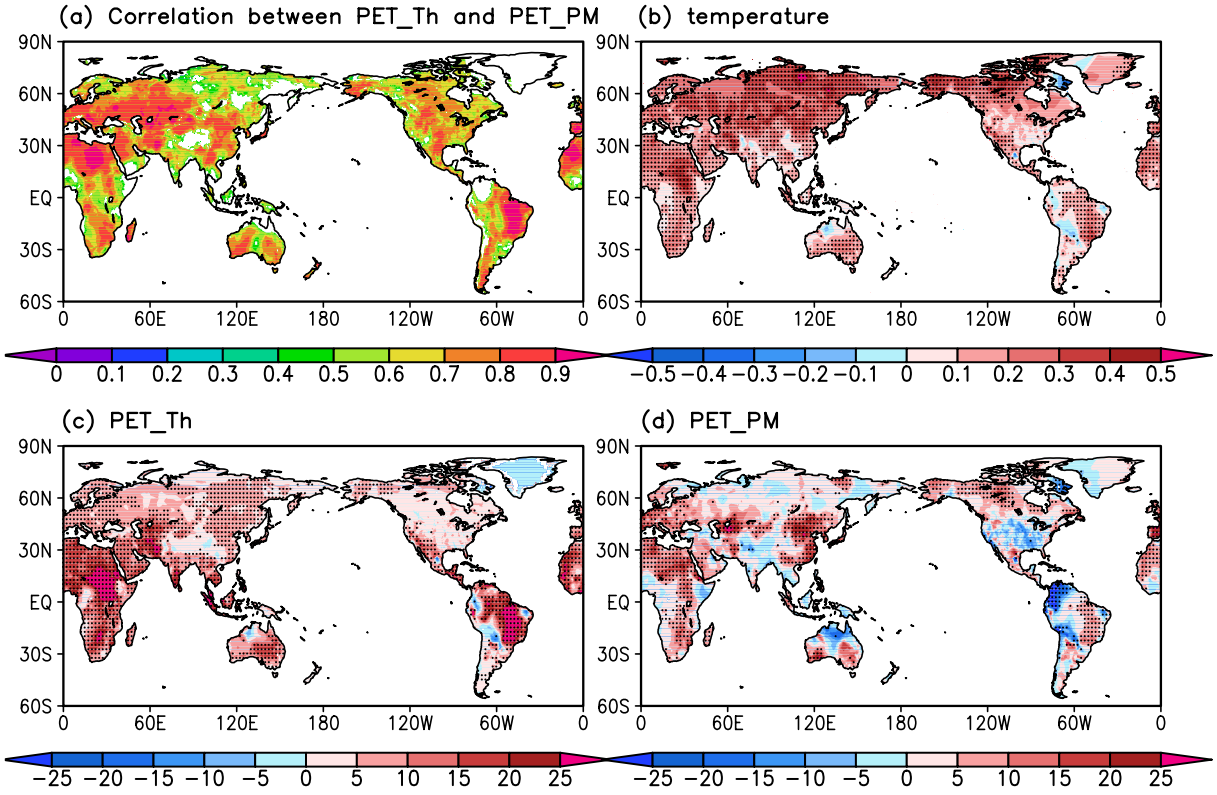

Fig. 3. (a) Correlation between PET_Th and PET_PM for the period 1951–2014. Shaded areas denote correlation coefficients statistically significant at the 0.001 level. (b–d) Long-term tendencies from 1951 to 2014 for (b) annual mean air temperature [units: °C (10 yr)$^{-1}$], (c) annual accumulated PET_Th and (d) PET_PM [units: mm (10 yr)$^{-1}$]. Stippling indicates the trend is statistically significant at the 0.001 level.

Table 2. Statistical values of annual accumulated PET_Th and PET_PM over northern South America, the USA, North Australia, and Central Asia. Difference means PET_PM minus PET_Th.

	1951–2014 mean (mm)			1901 (1951)–2014 linear trend [mm (10 yr)$^{-1}$]		1901 (1951)–2014
	PET_Th	PET_PM	Difference	PET_Th	PET_PM	correlation coefficient
South America	1460.7	1243.6	−217.1*	4.7* (10.2*)	−2.5* (−15.0*)	0.1 (0.1)
USA	791.3	1290.0	498.7*	2.5* (4.9*)	−1.0 (−3.0)	0.6* (0.5*)
North Australia	1477.7	2316.0	838.3*	2.5* (6.3*)	−6.5* (−6.9)	0.4* (0.4*)
Central Asia	1055.0	1341.1	286.1*	2.5* (5.1*)	−1.5* (−2.3)	0.5* (0.5*)

*Indicates difference, linear trend or correlation coefficient is statistically significant at the 0.05 level.

spatial extents and sizes for each arid region were obviously different. As shown in Fig. 6, drylands classified by SWI_PM and SWI_Th accounted for approximately 44.8% and 40.4%, respectively, of the global land area. Most drylands were distributed within the subtropics, where the underestimation of PET_Th resulted in larger SWI_Th and, consequently, fewer areas were classified as drylands. Between the classifications of SWI_Th and SWI_PM, differences in the areal percentages of drylands (4.4%) mainly derived from that in arid regions (4.1%). Although the areal percentages of semi-arid regions were approximately equal, their spatial extents were obviously different. It was apparent that high northern latitudes, where PET_Th was overestimated (Fig. 1c and Fig. 2), were classified as semi-arid and dry sub-humid regions by SWI_Th (Fig. 5a). This is not a reasonable result.

Consistent with the above results, more areas were defined as drylands by SWI_PM than by SWI_Th in all continents, excluding Antarctica (Fig. 6). For instance, drylands percentage classified by SWI_PM (16.8%) was twice that by SWI_Th (8.4%) over Europe. The spatial extent of drylands classified by SWI_ PM and SWI_Th in Oceania was the largest among the continents, at approximately 86.1% and 77.7%, respectively. Half of Oceania (51.4%) was classified as arid regions by SWI_ PM, whereas only 18.2% of the continental area was classified as arid regions by SWI_Th, which yielded a relatively wetter result because of the underestimation of PET. In Africa, the severity of aridity was the greatest among the continents, although the spatial extent of drylands was only second largest. Most of the world's hyper-arid regions were found to be concentrated within Africa, with

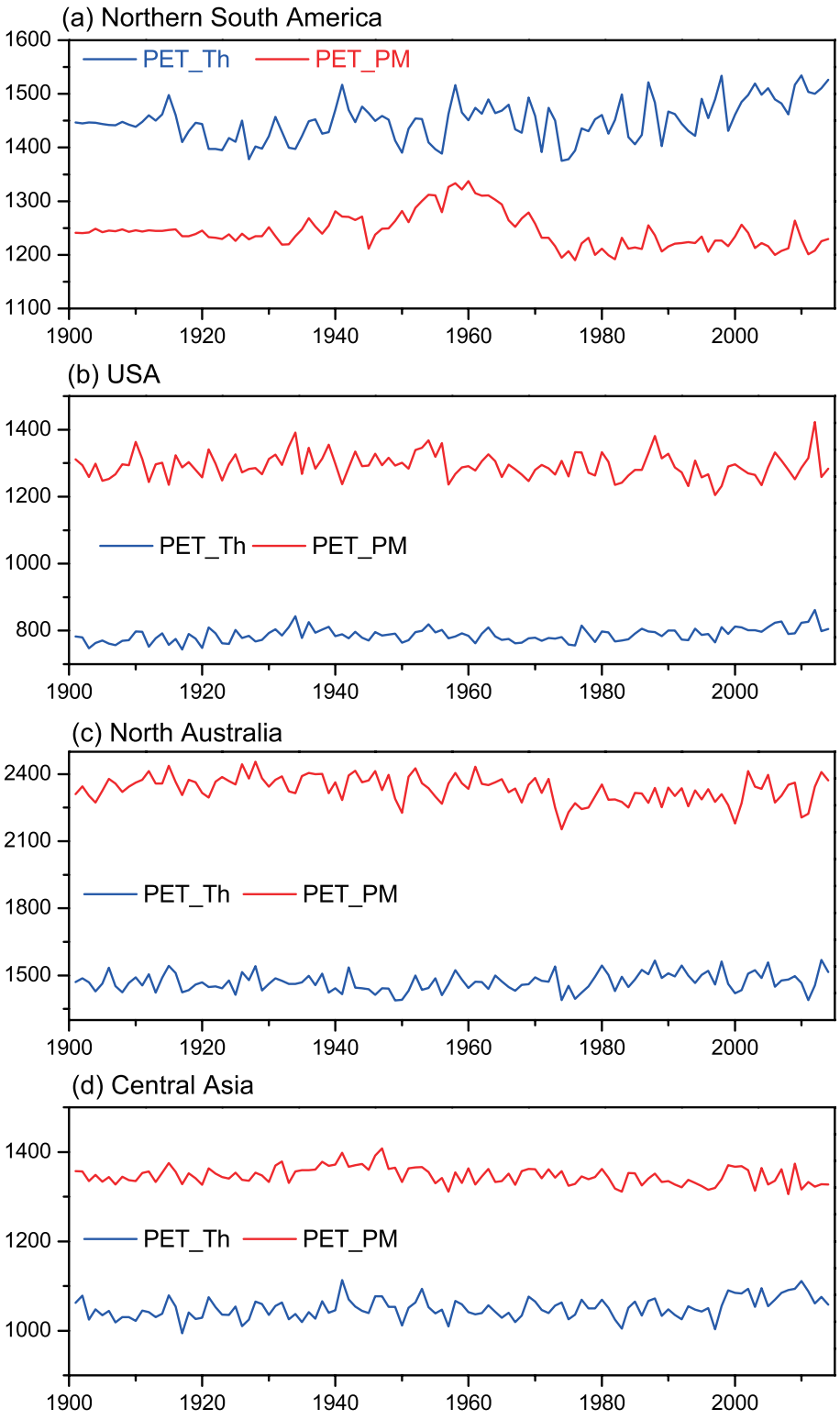

Fig. 4. Evolution of annual accumulated PET_Th and PET_PM (units: mm) from 1901 to 2014 over (a) northern South America (5°S–11°N, 60°–80°W), (b) USA (30°–45°N, 80°–120°W), (c) North Australia (23°–12°S, 120°–150°E) and (d) Central Asia (25°–38°N, 70°–80°E).

23.1% and 20.0% of the continental area classified as hyper-arid regions by SWI_ PM and SWI_Th, respectively. In Asia, only 3.2% of the continental area was classified as hyper-arid regions by SWI_Th, which is an obvious underestimation, i.e., the Taklamakan Desert in northwestern China should be classified as hyper-arid regions rather than arid regions. In North America, the semi-arid area based on SWI_Th comprised the north of Alaska and northern Canada instead of

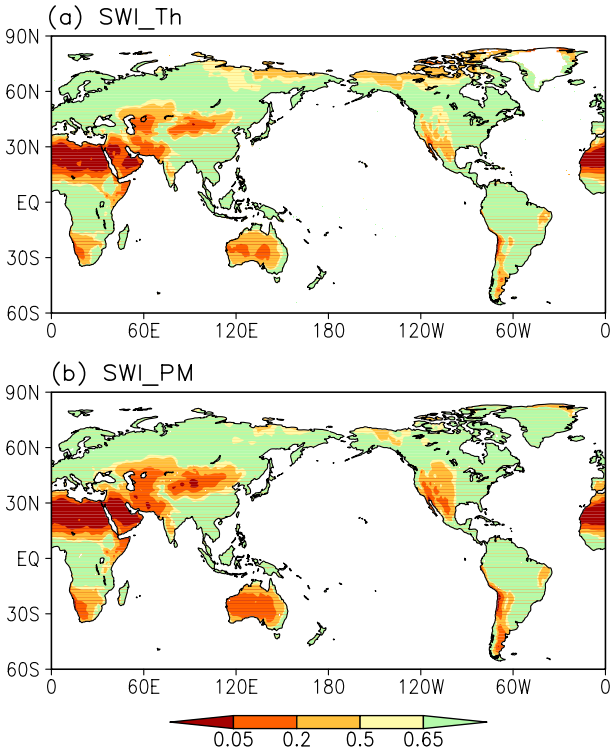

Fig. 5. Spatial distributions of global drylands using the 1951–2014 average: (a) SWI_Th; (b) SWI_PM.

most of the western United States. In South America, the distributions of drylands defined by SWI_PM and SWI_Th were similar; however, the sizes of each arid region based on SWI_Th were relatively smaller.

It is known that vegetation species respond not only to surface moisture conditions but also to effective cumulative temperature, soils, geomorphological and topographical features, and human activities. Therefore, surface vegetation types do not always match climatic zones exactly. As the main land cover type in hyper-arid and arid areas, the response of barren land to surface moisture deficit is much stronger and more durable with respect to other vegetation types. This is because of its short-term (months to years) resistance to change due to climatic variations and/or human activities. Generally, barren land tends to occur in drylands and drier regions have more barren land. As classified based on SWI_Th (Table 3), approximately 34.3%, 39.2%, 16.3% and 2.9% of global barren land was located in hyper-arid, arid, semi-arid and dry sub-humid regions, respectively. Of note is that the areal percentage of global barren land in arid regions (39.2%) was slightly larger than that in hyper-arid regions (34.3%), and more than half (62.4%) of areas were barren land in arid regions. For SWI_PM, global barren land was mainly concentrated in hyper-arid regions, with an areal percentage of 44.5%, and areal percentages of barren land declined sharply in regions with decreasing severity of aridity, ranging from 39.4% (arid regions) to 1.3% (dry sub-humid regions). Compared with SWI_Th-based

Table 3. Areal percentages of global barren land (P_1) located in hyper-arid, arid, semi-arid, and dry sub-humid regions, and areal percentages of barren land (P_2) over each arid region using 1951–2014 averages of SWI_Th and SWI_PM*.

		Hyper-arid	Arid	Semi-arid	Dry sub-humid
SWI_Th	P_1	34.3	39.2	16.3	2.9
	P_2	93.5	62.4	12.0	3.6
SWI_PM	P_1	44.5	39.4	9.2	1.3
	P_2	95.4	46.5	8.1	2.3

*$P_{1i} = a_i/(\sum_{i=1}^{5} a_i)\times 100\%$; $P_{2i} = a_i/b_i \times 100\%$, where a_i is the area of barren land in each climate zone, $i = 1,\ldots,5$ indicates hyper-arid, arid, semi-arid, dry sub-humid and humid regions, respectively, and then $\sum_{i=1}^{5} a_i$ represents the total area of global barren land; b_i is the area of each climate zone.

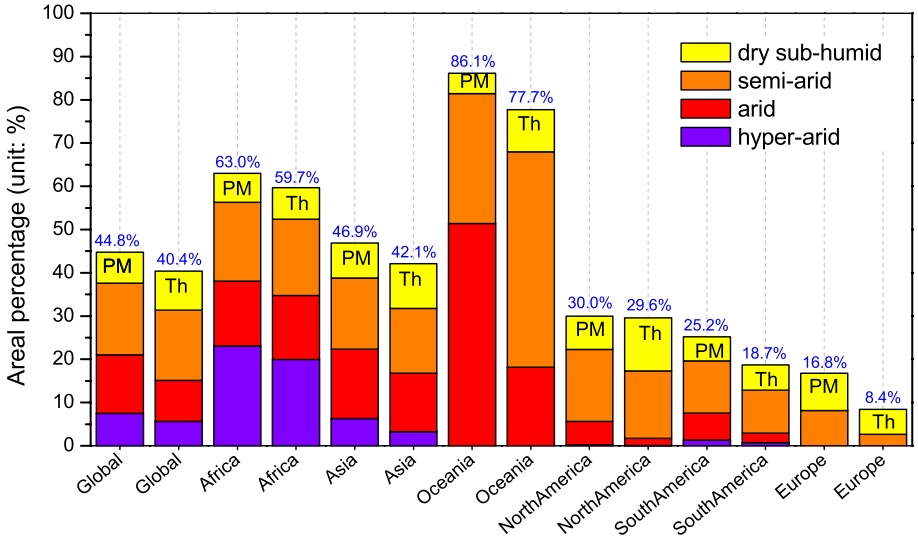

Fig. 6. Areal percentages of hyper-arid, arid, semi-arid, and dry sub-humid regions, using the 1951–2014 average SWI_Th and SWI_PM, respectively, over global and continental land areas. The blue number above each column indicates the areal percentage of drylands.

classification, hyper-arid regions defined by SWI_PM had more barren land (95.4%), whereas arid regions had less barren land (46.5%). Thus, SWI_PM presents a more reasonable and reliable spatial distribution of global drylands with respect to SWI_Th.

4.2. *Variability in temporal evolution*

Differences in the interdecadal variabilities of global drylands classified by SWI_Th and SWI_PM were compared on global and continental scales, after variations shorter than 20 years were removed using the EEMD method. Additionally, to quantitatively assess the contributions of precipitation and PET variations to dryland changes, dryland evolutions caused by precipitation or PET changes only are discussed separately.

4.2.1. *Global mean*

Figure 7a shows the interdecadal variabilities of areal percentages of global hyper-arid regions. Although there are differences among the curves, a sharp upward trend is evident during 1901–2014. Hyper-arid region evolutions caused by precipitation changes only presented similar interdecadal characteristics to those caused by both precipitation and PET changes, while those caused by PET_Th-only and PET_PM-

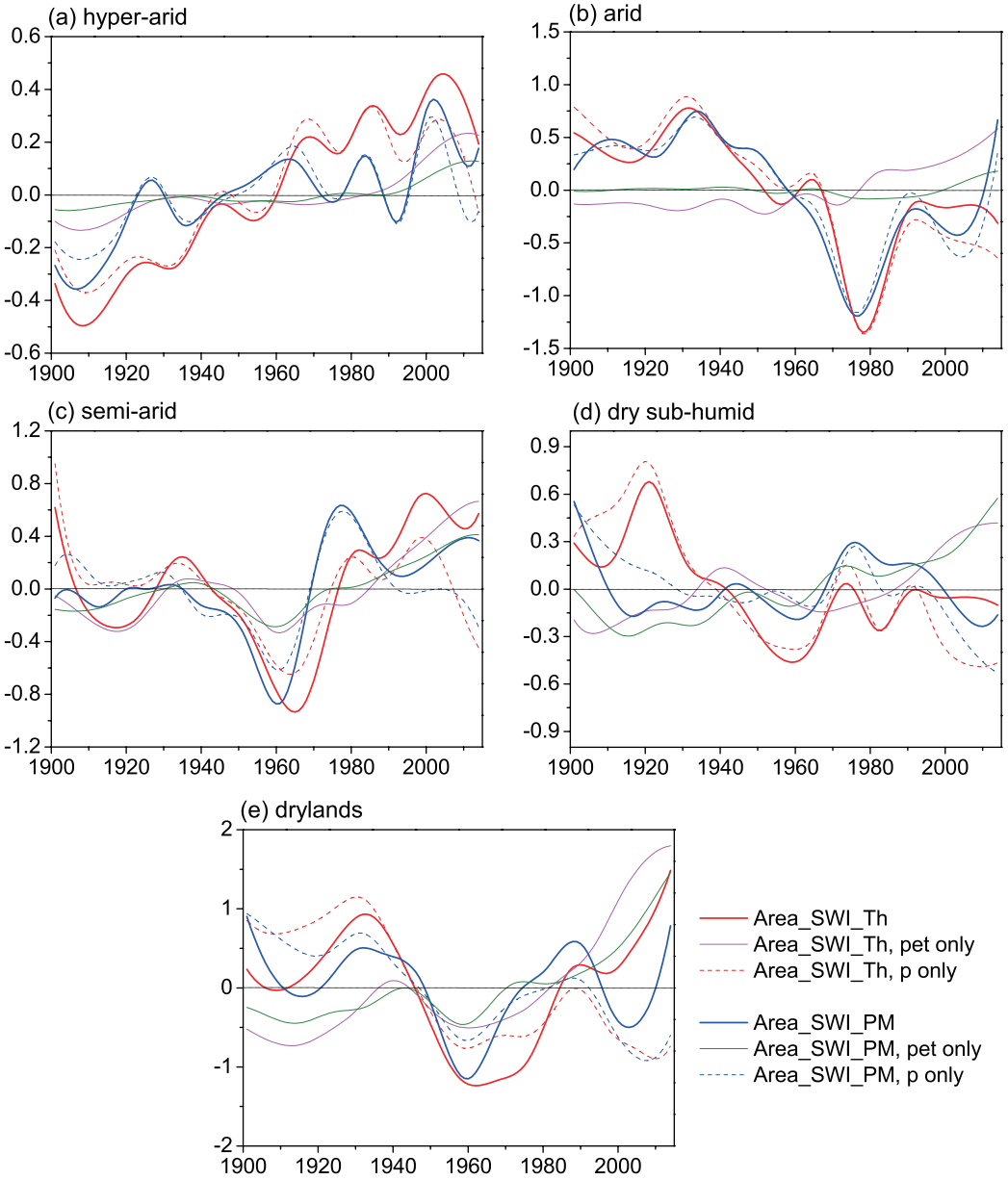

Fig. 7. Areal percentages (units: %) of global (a) hyper-arid, (b) arid, (c) semi-arid, (d) dry sub-humid regions, and (e) drylands during 1901–2014, defined by SWI_Th and SWI_PM, together with SWI_Th and SWI_PM with precipitation only (no PET changes, denoted by "p only") or PET only (no precipitation changes, denoted by "pet only").

only changes both showed a sustained upward trend since 1901, especially after the 1980s, in response to global warming. From the mid-1980s, the areal percentage of hyper-arid regions defined by SWI_Th exhibited a distinct interdecadal fluctuation without a long-term trend, whereas that defined by SWI_Th with precipitation changes only showed a significant downward trend. For the areal percentage of hyper-arid regions defined by SWI_PM, there was an obvious upward trend since the mid-1980s, whereas interdecadal fluctuation was apparent in that defined by SWI_PM with precipitation changes only. These findings indicate a global expansion of hyper-arid regions over the past 100 years, and the trend is insensitive to the two estimates for PET. Also of note is that the result of SWI_Th showed a greater (twice as large) upward trend [0.085% (10 yr^{-1})] than that of SWI_PM [0.040% (10 yr^{-1})]. Therefore, the global expansion of hyper-arid regions can be attributed to both increasing PET and decreasing precipitation, with the latter's contribution being approximately 70.9% and 61.6% in SWI_Th and SWI_PM, respectively.

The areal percentages of global arid regions (Fig. 7b) defined by SWI_Th and SWI_PM had similar variations, with a high correlation coefficient of 0.91 (Table 4). They both showed a significant downward trend during 1901–2014, at −0.104% $(10\ yr)^{-1}$ and −0.102% $(10\ yr)^{-1}$ respectively, and a shift from a positive to negative anomaly in the 1960s, as did those defined by precipitation changes only. However, arid region evolutions caused by PET_Th-only and PET_PM-only changes both showed a rising trend, and the upward trend of the former was statistically significant. This suggested that the areal percentages of global arid regions declined significantly during 1901–2014, because of the increases in precipitation, without obvious differences between the two estimates for PET. With respect to increasing PET, increasing precipitation plays a dominant role, which offsets the drying effect of increasing PET and eventually results in the contraction of arid regions. However, the expansion of arid regions was visible since the late 1970s because of both decreasing precipitation and increasing PET.

As shown in Fig. 7c, consistent with SWI_Th and SWI_PM, the SWI with PET_Th-only and PET_PM-only changes showed that a significant rising trend existed in the areal percentages of global semi-arid regions during 1901–2014, with an accelerated upward trend since the 1960s (Huang et al., 2016b). However, a weak declining trend was found in semi-arid region evolutions caused by precipitation changes only. This finding indicates that the dominant contributor to the expansion of global semi-arid regions is increasing PET, especially since the 1960s.

Table 4. Correlation coefficients (R) between interdecadal variations of each arid region defined by SWI_PM and SWI_PM over global and continental areas.

R	Hyper-arid	Arid	Semi-arid	Dry sub-humid	Dryland
Global	0.82*	0.91*	0.67*	0.03	0.66*
Asia	0.92*	0.92*	0.73*	0.20	0.78*
Africa	0.87*	0.81*	0.49*	0.27*	0.89*
Europe	–	–	0.74*	0.14	0.84*
North America	0.96*	0.78*	−0.11	0.12	0.58*
Oceania	0.84*	0.80*	0.68*	0.83*	0.80*
South America	0.39*	0.82*	0.77*	0.59*	0.80*

*Indicates correlation coefficient is statistically significant at the 0.01 level.

Areal percentages of global dry sub-humid regions (Fig. 7d) defined by SWI_Th and SWI_Th with precipitation changes only both presented a shift from a positive to negative anomaly in the early 1940s and a significant declining trend during 1901–2014. Also, the tendency for dry sub-humid region evolutions caused by precipitation changes only, i.e., −0.090% $(10\ yr)^{-1}$, was approximately twice that caused by both precipitation and PET_Th changes [−0.045% $(10\ yr)^{-1}$]. For the areal percentages of dry sub-humid regions defined by SWI_PM, obvious interdecadal fluctuation and an insignificant downward trend existed, whereas significant rising and declining trends were found in dry sub-humid region evolutions caused by PET_PM-only and precipitation-only changes, at 0.057% $(10\ yr)^{-1}$ and −0.043% $(10\ yr)^{-1}$, respectively. Notably, dry sub-humid region evolutions associated with SWI_PM differed considerably from those associated with SWI_Th, with a correlation coefficient of only 0.03 (Table 4); although, they both showed a contraction of global dry sub-humid regions that could be attributed to increases in precipitation. The contribution of increasing precipitation was approximately twice that of increasing PET in the evolution of dry sub-humid regions defined by SWI_Th, whereas the contributions of increasing precipitation and increasing PET approximately offset each other in that defined by SWI_PM.

Figure 7e shows the interdecadal variabilities of global drylands were broadly analogous to those of global semi-arid regions (Fig. 7c), which accounted for approximately 40.2% and 37.0% of global drylands defined by SWI_Th and SWI_PM, respectively. Distinct interdecadal fluctuations were presented clearly in dryland evolutions based on both SWI_Th and SWI_PM during 1901–2014. The evolutions of drylands caused by PET_Th-only and PET_PM-only changes both showed a significant rising trend, whereas a significant declining trend was exhibited in that caused by precipitation changes only, with a shift from a positive to negative anomaly during the 1940s. These results indicate the wetting effect of increasing precipitation approximately offsets the drying effect of increasing PET, resulting in no obvious long-term trend in global drylands defined by SWI_Th and a weak declining trend in that defined by SWI_PM.

Generally, the interdecadal variabilities of global drylands, including each arid region, were broadly similar between the classification of SWI_Th and SWI_PM, with high correlation coefficients ranging from 0.66 to 0.91; although, several differences existed in dry sub-humid regions, with a correlation coefficient of only 0.03. They both showed expansion of global hyper-arid and semi-arid regions, contraction of arid and dry sub-humid regions, and interdecadal fluctuation of drylands, during 1901–2014. This is because precipitation changes make a major contribution in the interdecadal

variabilities of global drylands, whereas PET changes contribute to a much lesser degree except in semi-arid regions. However, the contribution of PET changes has evidently increased since the 1980s, in response to global warming.

4.2.2. *Continental mean*

Figure 8a shows distinct interdecadal fluctuations in areal percentages of drylands over Asia defined by SWI_Th and SWI_PM during 1901–2014. A shift from a positive to negative anomaly occurred during the early 1940s, followed by a transition from a negative to positive anomaly during the late 1960s and early 1970s, and a reversal to a negative anomaly during the late 2000s. A significant upward trend was found in dryland evolutions caused by PET_Th-only and PET_PM-only changes, whereas that caused by precipitation-only changes presented a significant declining trend, and

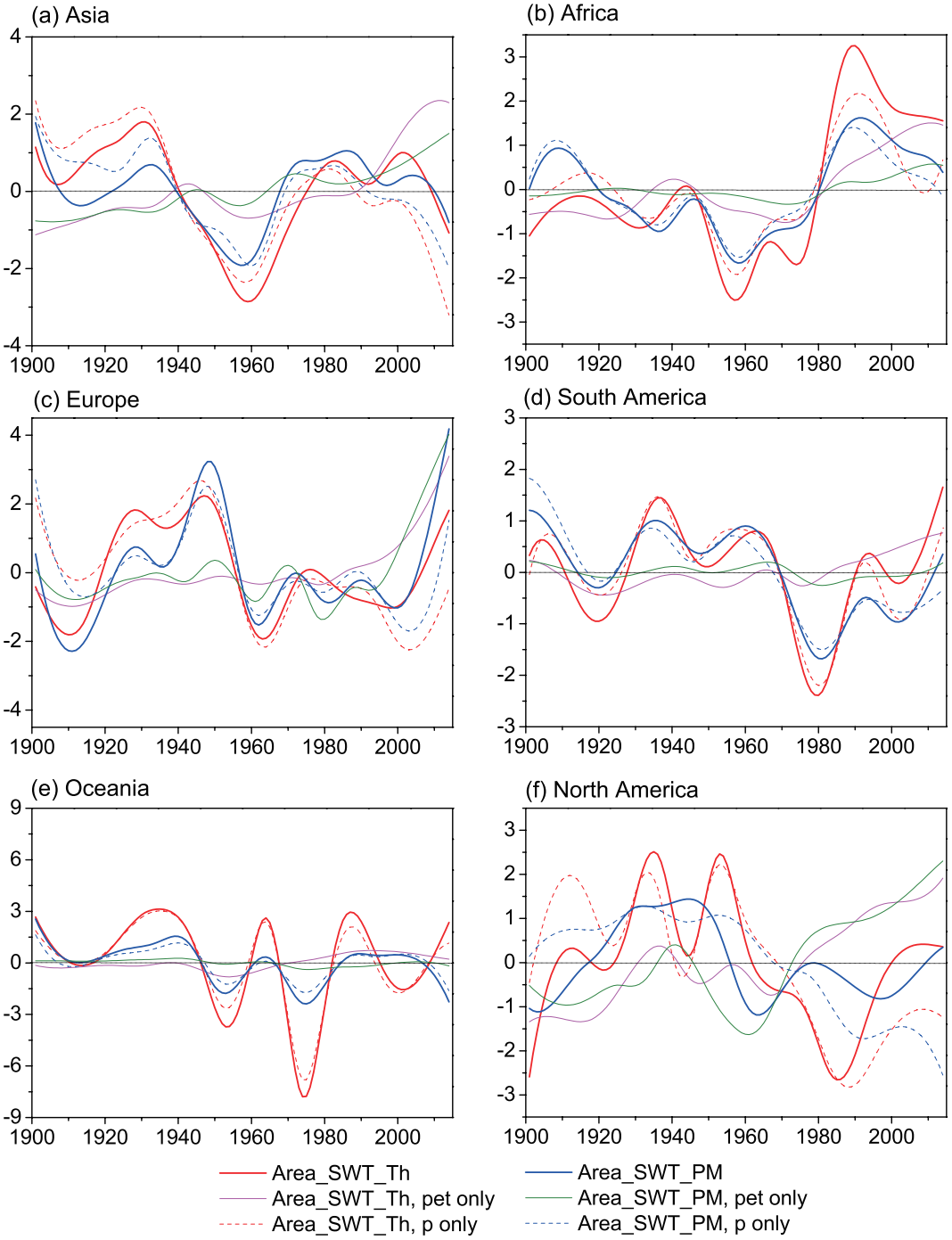

Fig. 8. Areal percentages (units: %) of drylands over (a) Asia, (b) Africa, (c) Europe, (d) South America, (e) Oceania, and (f) North America during 1901–2014, defined by SWI_Th and SWI_PM, together with SWI_Th and SWI_PM with precipitation only (no PET changes, denoted by "p only") or PET only (no precipitation changes, denoted by "pet only").

the tendency in the areal percentage of drylands defined by SWI_Th with precipitation-only changes was approximately twice that defined by SWI_PM with precipitation-only changes. After the 1980s, an accelerated upward trend in dryland evolutions caused by PET_Th-only and PET_PM-only changes was evident, as were enhanced differences between the evolutions of drylands defined by SWI_Th and SWI_Th with precipitation-only changes, as well as SWI_PM and SWI_PM with precipitation-only changes. This means that the influence of PET changes on drylands over Asia has intensified since the 1980s.

Unlike in Asia, an obvious upward trend was evident in the areal percentages of drylands over Africa, especially since the late 1950s, with a shift from a negative to positive anomaly during the late 1970s and early 1980s, albeit with some differences among the curves apparent (Fig. 8b). These trends could be attributed to sustained decreasing precipitation since the late 1950s and increasing PET since the 1970s. The contributions of PET changes accounted for approximately 60.4% in the evolutions of drylands defined by SWI_Th, and approximately 51.1% in those defined by SWI_PM. It has also been noted that a declining trend existed in dryland changes during the early 1990s because of substantially increased precipitation across the Sahel and southern Africa (Maidment et al., 2015).

Among the continents, Europe had the smallest areal percentage of drylands, containing no hyper-arid or arid regions (Fig. 6). Both SWI_Th and SWI_PM showed obvious interdecadal fluctuations in the evolutions of drylands over Europe during 1901–2014 (Fig. 8c). Two transitions from a negative to positive anomaly occurred during the early 1920s and the mid-2000s, respectively, and a shift from a positive to negative anomaly appeared during the mid-1950s. In contrast to the sustained upward trend in dryland changes caused by PET_Th-only changes, that induced by PET_PM-only changes showed similar interdecadal fluctuations to the evolutions of drylands defined by SWI_PM and SWI_PM with precipitation-only changes. Since the early 2000s, a sharply rising trend was evident among all curves, which could be attributed to decreasing precipitation plus increasing PET.

As shown in Fig. 8d, interdecadal variabilities of drylands over South America were analogous to those over Europe in terms of cycle and transitions. It was noted that a significant upward trend was apparent in dryland evolutions caused by PET_Th-only changes, whereas that caused by PET_PM-only changes presented a significant downward trend. This was because PET_Th and PET_PM had opposite long-term trends over South America, i.e., a significant upward and downward trend, respectively (Table 2). The wetting effect of increasing precipitation was partly offset and, consequently, there was no distinct long-term trend in the evolutions of drylands defined by SWI_Th; whereas, the wetting effect of increasing precipitation was enhanced and significant contraction of drylands was associated with SWI_PM-based classification.

For the evolutions of drylands over Oceania (Fig. 8e), consistent interdecadal fluctuations with a downward trend were shown in SWI_Th, SWI_PM and those with precipitation-only changes. However, areal percentages of drylands defined by SWI_Th and SWI_Th with precipitation-only changes had a larger amplitude, and their fluctuations were out of phase with those defined by SWI_PM and SWI_PM with precipitation-only changes since the mid-1990s. Consistent with South America, opposing long-term trends of the two estimates for PET were also found. This finding indicates that precipitation changes dominate the interdecadal variabilities of drylands and the contribution of PET changes is relatively less.

In contrast to the other continents, there were distinct differences between the evolutions of drylands defined by SWI_Th and SWI_PM over North America; although, a declining trend was shown in both (Fig. 8f). In the classification of SWI_PM, obvious interdecadal fluctuations were found, with two transitions from a negative to positive anomaly, and from a positive to negative anomaly, during the late 1910s and the mid-1950s, respectively. However, areal percentages of drylands defined by SWI_Th showed relatively higher frequency variations and an opposing long-term trend since the mid-1960s. This was because high northern latitudes over North America were classified as humid regions by SWI_PM, but as semi-arid and dry sub-humid regions by SWI_Th (Fig. 5a). Consequently, the areal percentages of semi-arid (dry sub-humid) regions defined by SWI_Th and SWI_PM showed distinct differences during 1901–2014, with a correlation coefficient of only −0.11 (0.12) (Table 4). Also of note was that the interdecadal variations in drylands caused by PET_PM-only changes were comparable with those defined by SWI_PM and SWI_PM with precipitation-only changes, in terms of amplitude and long-term trends, and this was also true in the classification of the three kinds of SWI_Th. This means that the contributions of precipitation and PET changes are approximately equal and offset each other over North America.

Besides North America, the interdecadal variations of drylands defined by SWI_PM and SWI_PM were analogous and reasonably comparable among the continents, with high correlation coefficients ranging from 0.58 to 0.89 (Table 4). This was because precipitation changes made a major contribution to the interdecadal variabilities of drylands over each continent. Also of note was that the spatial extent of the climatic dry–wet transition zone was very sensitive to PET values, and thus differences attributable to the two estimates for PET tended to manifest there.

5. Discussion and conclusions

PET represents the maximum amount of water capable of being lost from the land surface, and is a critical component of the land water cycle and an important input to the SWI in defining global drylands. The Thornthwaite method is a popular way to estimate PET because of the simplicity of the computations required and the minimal demand regarding meteorological variables. The Penman–Monteith method is considered more realistic physically, but it requires some ad-

ditional meteorological variables. Various estimates of PET in the SWI will certainly induce different classifications of global drylands. Therefore, the present study assessed the sensitivity of the SWI to the two estimates for PET, in the study of the spatial distributions and temporal evolutions of global drylands, especially on interdecadal timescales, for the purpose of providing background and information helpful in selecting an appropriate PET parameterization in the analysis of global drylands.

Considerable differences were found between the two kinds of PET. In terms of spatial extent, the differences exhibited distinct zonal characteristics. With respect to PET_PM, PET_Th was significantly lower in the subtropics, whereas it was significantly higher in the tropics and high northern latitudes. This is because the Thornthwaite-based PET cannot capture the influence of solar radiation, vapor pressure deficit, and wind speed. Because most drylands are distributed within the subtropics, the underestimation of PET by the Thornthwaite method in this region results in fewer areas being classified as drylands on global and continental scales. The classifications given by SWI_PM and SWI_Th showed drylands as covering approximately 44.8% and 40.4% of the global land area, respectively. In terms of long-term trends, PET_Th exhibited a direct response to the effects of global warming, and showed a significant rising trend over most global land areas. In contrast, regions with increasing PET_PM and global warming both only accounted for approximately 47% of theglobal land area, excluding Antarctica. Compared with SWI_Th, SWI_PM presented a more reasonable and reliable spatial distribution of global drylands, which could be confirmed by the global distribution of barren land.

Besides North America, broadly similar results, with high correlation coefficients ranging from 0.58 to 0.89, were presented in the interdecadal variabilities of global drylands defined by SWI_PM and SWI_Th. Global expansion of hyperarid and semi-arid regions, contraction of arid and dry subhumid regions, and interdecadal fluctuation of drylands, were evident during 1901–2014, and these trends were not very sensitive to differences between the two estimates for PET. This is because precipitation changes make a major contribution in the interdecadal variabilities of drylands, whereas PET changes contribute to a lesser degree. For North America, the spatial extent of drylands defined by SWI_Th was obviously different from that defined by SWI_PM. The north of Alaska and northern Canada, instead of most of the western United States, were classified as semi-arid and dry sub-humid regions by SWI_Th. Consequently, SWI_Th failed to provide a reasonable result for the interdecadal variations in drylands over North America. Additionally, it should be noted that the influences of PET changes on the interdecadal variabilities of semi-arid and dry sub-humid regions were comparable to those of precipitation changes, and thus estimates of PET based on the different methods could yield diverse results.

It has been noted that the influences of PET changes on the interdecadal variabilities of global drylands have gradually enhanced with global warming. The response of drylands to PET variations in the future could be significantly different from that over the past 100 years. Compared with the Thornthwaite method, the Penman–Monteith method is recommended in the analysis of global drylands in the future, especially in the climatic dry–wet transition zone. Additionally, the applicability of some minimalistic PET models, such as a simplified equation developed by Hargreaves and Allen (2003), which can provide very similar estimates to the Penman–Monteith method, in the analysis of global drylands, has yet to be further investigated but should be addressed in future work.

Acknowledgements. This study was jointly sponsored by the National K&D Program of China (Grant No. 2016YFA0600404), the China Special Fund for Meteorological Research in the Public Interest (Grant No. GYHY201106028 and GYHY201506001-1), the National Natural Science Foundation of China (Grant No. 41530532), and the Jiangsu Collaborative Innovation Center for Climate Change.

REFERENCES

Allen, R. G., M. Smith, A. Perrier, and L. S. Pereira, 1994a: An update for the definition of reference evapotranspiration. *ICID Bulletin*, **43**, 1–34.

Allen, R. G., M. Smith, A. Perrier, and L. S. Pereira, 1994b: An update for the calculation of reference evapotranspiration. *ICID Bulletin*, **43**, 35–92.

An, L. J., F. M. Ren, Y. J. Li, and Y. P. Li, 2014: Study on characteristics of regional drought events over north China during the past 50 years. *Meteorological Monthly*, **40**, 1097–1105, doi: 10.7519/j.issn.1000-0526.2014.09.007. (in Chinese with English abstract)

Beguería, S., S. M. Vicente-Serrano, F. Reig, and B. Latorre, 2014: Standardized precipitation evapotranspiration index (SPEI) revisited: Parameter fitting, evapotranspiration models, tools, datasets and drought monitoring. *International Journal of Climatology*, **34**, 3001–3023, doi: 10.1002/joc.3887.

Bontemps, S., P. Defourny, E. Van Bogaert, O. Arino, V. Kalagirou, and J. R. Perez, 2011: GlobCover 2009: Products description and validation report. [Available online from http://ionia1.esrin.esa.int/docs/GLOBCOVER2009_Validation_Report_2.]

Cong, Z. T., D. W. Yang, and G. H. Ni, 2009: Does evaporation paradox exist in China? *Hydrology and Earth System Sciences*, **13**, 357–366.

Dai, A. G., 2011: Characteristics and trends in various forms of the Palmer Drought Severity Index during 1900-2008. *J. Geophys. Res.*, **116**, D12115, doi: 10.1029/2010JD015541.

Dai, A. G., 2013: Increasing drought under global warming in observations and models. *Nat. Clim. Change*, **3**, 52–58, doi:10.1038/nclimate1633.

Feng, S., and Q. Fu, 2013: Expansion of global drylands under a warming climate. *Atmospheric Chemistry and Physics*, **13**, 10 081–10 094, doi: 10.5194/acp-13-10081-2013.

Feng, S., M. Trnka, M. Hayes, and Y. J. Zhang, 2017: Why do different drought indices show distinct future drought risk outcomes in the U.S. great plains? *J. Climate*, **30**, 265–278, doi: 10.1175/JCLI-D-15-0590.1.

Food and Agriculture Organization of the United Nations, 2008:

Water and cereals in drylands. Food and Agriculture Organization of the United Nations, Roma.

Fu, G. B., S. P. Charles, and J. J. Yu, 2009: A critical overview of pan evaporation trends over the last 50 years. *Climatic Change*, **97**, 193–214, doi: 10.1007/s10584-009-9579-1.

Gao, G., D. L. Chen, G. Y. Ren, Y. Chen, and Y. M. Liao, 2006: Spatial and temporal variations and controlling factors of potential evapotranspiration in China: 1956-2000. *Journal of Geographical Sciences*, **16**, 3–12, doi: 10.1007/s11442-006-0101-7.

Gao, G., D. L. Chen, C.-Y. Xu, and E. Simelton, 2007: Trend of estimated actual evapotranspiration over China during 1960-2002. *J. Geophys. Res.*, **112**, D11120, doi: 10.1029/2006JD008010.

Hargreaves, G. H., and R. G. Allen, 2003: History and Evaluation of Hargreaves Evapotranspiration Equation. *Journal of Irrigation and Drainage Engineering*, **129**, 53–63, doi: 10.1061/(ASCE)0733-9437(2003)129:1(53).

Harris, I., P. D. Jones, T. J. Osborn, and D. H. Lister, 2014: Updated high-resolution grids of monthly climatic observations-the CRU TS3.10 Dataset. *International Journal of Climatology*, **34**, 623–642, doi: 10.1002/joc.3711.

Heim, R. R., Jr., 2002: A review of twentieth-century drought indices used in the United States. *Bull. Amer. Meteor. Soc.*, **83**, 1149–1165, doi: 10.1175/1520-0477(2002)083<1149:AROTDI>2.3.CO;2.

Huang, J. P., H. P. Yu, X. D. Guan, G. Y. Wang, and R. X. Guo, 2016a: Accelerated dryland expansion under climate change. *Nat. Clim. Change*, **6**, 166–171, doi: 10.1038/nclimate2837.

Huang, J. P., M. X. Ji, Y. K. Xie, S. S. Wang, Y. L. He, and J. J. Ran, 2016b: Global semi-arid climate change over last 60 years. *Climate Dyn.*, **46**, 1131–1150, doi: 10.1007/s00382-015-2636-8.

Huang, N. E., and Z. H. Wu, 2008: A review on Hilbert-Huang transform: Method and its applications to geophysical studies. *Rev. Geophys.*, **46**, RG2006, doi: 10.1029/2007RG000228.

Hulme, M., R. Marsh, and P. D. Jones, 1992: Global changes in a humidity index between 1931-60 and 1961-90. *Climate Research*, **2**, 1–22, doi: 10.3354/cr002001.

Keyantash, J., and J. A. Dracup, 2002: The quantification of drought: An evaluation of drought indices. *Bull. Amer. Meteor. Soc.*, **83**, 1167–1180, doi: 10.1175/1520-0477(2002)083<1191:TQODAE>2.3.CO;2.

Li, Y., J. P. Huang, M. X. Ji, and J. J. Ran, 2015: Dryland expansion in northern China from 1948 to 2008. *Adv. Atmos. Sci.*, **32**, 870–876, doi: 10.1007/s00376-014-4106-3.

Lioubimtseva, E., and G. M. Henebry, 2009: Climate and environmental change in arid Central Asia: Impacts, vulnerability, and adaptations. *Journal of Arid Environments*, **73**, 963–977, doi: 10.1016/j.jaridenv.2009.04.022.

Liu, B., and Z. G. Ma, 2007: Area change of dry and wet regions in China in the past 45 years. *Arid Land Geography*, **30**, 7–15, doi: 10.3321/j.issn:1000-6060.2007.01.002. (in Chinese with English abstract)

Ma, Z. G., and C. B. Fu, 2003: Interannual characteristics of the surface hydrological variables over the arid and semi-arid areas of northern China. *Global and Planetary Change*, **37**, 189–200, doi: 10.1016/S0921-8181(02)00203-5.

Ma, Z. G., and C. B. Fu, 2005: Decadal variations of arid and semi-arid boundary in China. *Chinese Journal of Geophysics*, **48**, 519–525, doi: 10.3321/j.issn:0001-5733.2005.03.008. (in Chinese with English abstract)

Ma, Z. G., and C. B. Fu, 2006: Some evidence of drying trend over northern China from 1951 to 2004. *Chinese Science Bulletin*, **51**, 2913–2925, doi: 10.1007/s11434-006-2159-0.

Ma, Z. G., and C. B. Fu, 2007: Global aridification in the second half of the 20th century and its relationship to large-scale climate background. *Science in China Series D: Earth Sciences*, **50**, 776–788, doi: 10.1007/s11430-007-0036-6.

Maidment, R. I., R. P. Allan, and E. Black, 2015: Recent observed and simulated changes in precipitation over Africa. *Geophys. Res. Lett.*, **42**, 8155–8164, doi: 10.1002/2015gl065765.

McMahon, T. A., B. L. Finlayson, and M. C. Peel, 2016: Historical developments of models for estimating evaporation using standard meteorological data. *Wiley Interdisciplinary Reviews: Water*, **3**, 788–818, doi: 10.1002/wat2.1172.

Mishra, A. K., and V. P. Singh, 2010: A review of drought concepts. *Journal of Hydrology*, **391**, 202–216, doi: 10.1016/j.jhydrol.2010.07.012.

Palmer, W. C., 1965: Meteorological drought. Research Paper No. 45. U.S. Weather Bureau, Washington, D.C.

Qian, C., and T. J. Zhou, 2014: Multidecadal variability of north China aridity and its relationship to PDO during 1900-2010. *J. Climate*, **27**, 1210–1222, doi: 10.1175/JCLI-D-13-00235.1.

Rezaei, M., M. Valipour, and M. Valipour, 2016: Modelling evapotranspiration to increase the accuracy of the estimations based on the climatic parameters. *Water Conservation Science and Engineering*, **1**, 197–207, doi: 10.1007/s41101-016-0013-z.

Reynolds, J. F., and Coauthors, 2007: Global desertification: Building a science for dryland development. *Science*, **316**, 847–851, doi: 10.1126/science.1131634.

Roderick, M. L. and G. D. Farquhar, 2002: The cause of decreased pan evaporation over the past 50 years. *Science*, **298**, 1410–1411.

Sheffield, J., E. F. Wood, and M. L. Roderick, 2012: Little change in global drought over the past 60 years. *Nature*, **491**, 435–438, doi: 10.1038/nature11575.

Sherwood, S., and Q. Fu, 2014: A drier future? *Science*, **343**, 737–739, doi: 10.1126/science.1247620.

Shuttleworth, W. J., and J. S. Wallace, 1985: Evaporation from sparse crops-An energy combination theory. *Quart. J. Roy. Meteor. Soc.*, **111**, 839–855, doi: 10.1002/qj.49711146910.

Tegos, A., N. Malamos, and D. Koutsoyiannis, 2015: A parsimonious regional parametric evapotranspiration model based on a simplification of the Penman-Monteith formula. *J. Hydrol.*, **524**, 708–717, doi: 10.1016/j.jhydrol.2015.03.024.

Thornthwaite, C. W., 1948: An approach toward a rational classification of climate. *Geographical Review*, **38**, 55–94, doi: 10.2307/210739.

Trenberth, K. E., A. G. Dai, G. van der Schrier, P. D. Jones, J. Barichivich, K. R. Briffa, and J. Sheffield, 2014: Global warming and changes in drought. *Nat. Clim. Change*, **4**, 17–22, doi: 10.1038/nclimate2067.

United Nations Environment Programme (UNEP), 1992: World atlas of desertification. Edward Arnold, Sevenoaks, 68pp.

Valipour, M., 2013: Use of surface water supply index to assessing of water resources management in Colorado and Oregon, US. *Advances in Agriculture, Sciences and Engineering Research*, **3**, 631–640.

Valipour, M., M. A. Gholami Sefidkouhi, and M. Raeini-Sarjaz, 2017: Selecting the best model to estimate potential evapotranspiration with respect to climate change and magnitudes

of extreme events. *Agricultural Water Management*, **180**, 50–60, doi: 10.1016/j.agwat.2016.08.025.

van der Schrier, G., P. D. Jones, and K. R. Briffa, 2011: The sensitivity of the PDSI to the Thornthwaite and Penman-Monteith parameterizations for potential evapotranspiration. *J. Geophys. Res.*, **116**, D03106, doi: 10.1029/2010JD015001.

van der Schrier, G., J. Barichivich, K. R. Briffa, and P. D. Jones, 2013: A scPDSI-based global data set of dry and wet spells for 1901-2009. *J. Geophys. Res.*, **118**, 4025–4048, doi: 10.1002/jgrd.50355.

Vicente-Serrano, S. M., S. Beguería, and J. I. López-Moreno, 2010a: A multiscalar drought index sensitive to global warming: The standardized precipitation evapotranspiration index. *J. Climate*, **23**, 1696–1718, doi: 10.1175/2009JCLI2909.1.

Vicente-Serrano, S. M., S. Beguería, J. I. López-Moreno, M. Angulo, and A. El Kenawy, 2010b: A new global 0.5° gridded dataset (1901–2006) of a multiscalar drought index: Comparison with current drought index datasets based on the palmer drought severity index. *Journal of Hydrometeorology*, **11**, 1033–1043, doi: 10.1175/2010JHM1224.1.

Vicente-Serrano, S. M., and Coauthors, 2012: Performance of drought indices for ecological, agricultural, and hydrological applications. *Earth Interactions*, **16**, 10, doi: 10.1175/2012EI000434.1.

Wilks, D. S., 2005: *Statistical Methods in the Atmospheric Sciences* (*International Geophysics*). 2nd ed. Academic Press.

Willmott, C. J., C. M. Rowe, and Y. Mintz, 1985: Climatology of the terrestrial seasonal water cycle. *J. Climatol.*, **5**, 589–606, doi: 10.1002/joc.3370050602.

Wu, Z. H., and N. E. Huang, 2009: Ensemble empirical mode decomposition: A noise-assisted data analysis method. *Advances in Adaptive Data Analysis*, **1**, 1–41, doi: 10.1142/S1793536909000047.

Wu, Z. H., N. E. Huang, J. M. Wallace, B. V. Smoliak, and X. Y. Chen, 2011: On the time-varying trend in global-mean surface temperature. *Climate Dyn.*, **37**, 759–773, doi: 10.1007/s00382-011-1128-8.

Xia, J. J., Z. W. Yan, and P. L. Wu, 2013: Multidecadal variability in local growing season during 1901-2009. *Climate Dyn.*, **41**, 295–305, doi: 10.1007/s00382-012-1438-5.

Xu, C.-Y., L. B. Gong, T. Jiang, D. L. Chen, and V. P. Singh, 2006: Analysis of spatial distribution and temporal trend of reference evapotranspiration and pan evaporation in Changjiang (Yangtze River) catchment. *J. Hydrol.*, **327**, 81–93, doi: 10.1016/j.jhydrol.2005.11.029.

Yuan, S. S., and S. M. Quiring, 2014: Drought in the U.S. great plains (1980-2012): A sensitivity study using different methods for estimating potential evapotranspiration in the Palmer Drought Severity Index. *J. Geophys. Res.*, **119**, 10 996–11 010, doi: 10.1002/2014JD021970.

Zhang, J., F. B. Sun, J. J. Xu, Y. N. Chen, Y.-F. Sang, and C. M. Liu, 2016: Dependence of trends in and sensitivity of drought over China (1961-2013) on potential evaporation model. *Geophys. Res. Lett.*, **43**, 206–213, doi: 10.1002/2015GL067473.

Zhou, M. C., H. Ishidaira, and K. Takeuchi, 2008: Comparative study of potential evapotranspiration and interception evaporation by land cover over Mekong basin. *Hydrological Processes*, **22**, 1290–1309, doi: 10.1002/hyp.6939.